physica status solidi pss rrl
www.pss-rapid.com

Check for updates

Electric Fields and Surface Fermi Level in Undoped GaN/AlN Two-Dimensional Hole Gas Heterostructures

Łukasz Janicki, Reet Chaudhuri, Samuel James Bader, Huili Grace Xing, Debdeep Jena, and Robert Kudrawiec*

Undoped GaN/AlN heterostructures with a high-density 2D hole gas (2DHG) have recently been reported, demonstrating that holes can be generated in GaN without magnesium (Mg) doping. The presence of the high-density 2DHG in these GaN/AlN heterostructures is expected to result from huge internal polarization fields. Herein, modulation spectroscopy is applied to analyze the built-in electric fields in the top GaN layer of molecular beam epitaxy (MBE)-grown GaN/AlN heterostructures with a buried 2DHG using contactless electroreflectance (CER). Experimentally obtained electric field values are compared with self-consistent Schrödinger–Poisson energy band calculations of the GaN/AlN structures. This coupled experimental and theoretical analysis determines that the Fermi level at the GaN surface is located at ≈1.9 above the valence band (i.e., roughly in the middle of the bandgap)—for structures with undoped and Mg-doped GaN. Finally, the comparison of calculated 2DHG concentrations in the structures under study with values determined from Hall effect measurements shows excellent agreement further strengthening the result.

1. Introduction

III-nitride-based p-channel devices have been studied with high interest in the past decade toward achieving complementary functionality to the ubiquitous n-channel AlGaN/GaN high-electron mobility transistors (HEMTs). Various heterostructures and devices with hole channels have been demonstrated toward this.[1–6] However, these structures either contain a parallel 2D electron channel or have low 2D hole gas (2DHG) densities limited by magnesium (Mg) doping and a polarization difference across alloy interfaces. Thanks to the advancement in AlN-as-substrate technology, record radio frequency p-channel FETs using a binary GaN/AlN structure have recently been reported,[7,8] which take advantage of the high polarization difference between GaN and AlN to obtain a high-density hole channel. Record high-conductivity 2DHGs in undoped metal-polar GaN/AlN heterostructures, the p-type analog of AlN/GaN 2DEGs, provide experimental evidence that holes can be obtained in a GaN channel without Mg doping.[9] The presence of the 2DHG at the GaN/AlN heterointerface points to the existence of a high built-in electric field in the top GaN layer due to the polarization. Probing and studying this electric field, and the subsequent physical phenomena associated with it, provide valuable information about the structure, including the surface Fermi level which is an important parameter toward a full understanding of the physics behind the 2DHG formation in these structures.

Electric fields in semiconductor thin films can be studied in an all-optical way using modulation spectroscopy techniques.[10] By applying a modulating field signal to the heterostructure either directly (electromodulation) or indirectly (contactless electroreflectance [CER] and photoreflectance), the complex dielectric constant of the film is varied, thereby giving rise to a change in the reflectance of an incident light beam. The resulting spectra contain Franz–Keldysh oscillations (FKO) that are dependent on the built-in electric field, thus making modulation spectroscopy a potent tool to study intrinsic electric fields and surface states. Such studies were first proposed for GaAs, based on a surface/intrinsic/n-doped (s–i–n) or surface/intrinsic/p-doped (s–i–p) Van Hoof structure stack,[11] and since then have been extended for other materials.[12,13] Using CER, where the electric field is modulated by placing the sample in a transparent capacitor setup, the surface Fermi level of GaN in air ambient has previously been shown to take two distinct positions—close to the conduction band or in middle of the bandgap, depending on the material conditions and structure design.[14]

Dr. Ł. Janicki, Prof. R. Kudrawiec
Department of Semiconductor Materials Engineering
Wrocław University of Science and Technology
Wybrzeże Wyspiańskiego 27, Wrocław 50-370, Poland
E-mail: lukasz.janicki@pwr.edu.pl

R. Chaudhuri, Prof. H. G. Xing, Prof. D. Jena
Electrical and Computer Engineering
Cornell University
Ithaca, NY 14853, USA

S. J. Bader
Applied and Engineering Physics
Cornell University
Ithaca, NY 14853, USA

Prof. H. G. Xing, Prof. D. Jena
Material Science and Engineering
Cornell University
Ithaca, NY 14853, USA

Prof. H. G. Xing, Prof. D. Jena
Kavli Institute of Nanoscale Science
Cornell University
Ithaca, NY 14853, USA

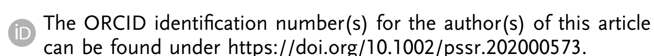
The ORCID identification number(s) for the author(s) of this article can be found under https://doi.org/10.1002/pssr.202000573.

DOI: 10.1002/pssr.202000573

 © 2021 Wiley-VCH GmbH

In this work, the CER technique is used to study metal-polar GaN/AlN heterostructures containing a high-density 2DHG. Due to the high built-in electric field in the top GaN layer, FKO were observed in the CER spectra. The FKOs were analyzed to quantitatively determine the electric field in GaN/AlN heterostructures with undoped GaN (≈0.6 MV cm^{-1}) and Mg-doped GaN (≈1.5 MV cm^{-1}). Self-consistent 1D Schrödinger–Poisson calculations were carried out for the band profiles of GaN/AlN structures, using the experimentally determined field in the GaN layer as a parameter. Through this coupled experimental and theoretical analysis, the surface Fermi level was derived to be ≈1.9 above the valence band (VB) (roughly in the middle of the bandgap) for both the structures, a result that is consistent with previous studies of the air–GaN interface by CER.[14] The comparison of calculated 2DHG concentrations in the structures under study with values determined from Hall effect measurements showed good agreement further strengthening the result.

2. Results and Discussion

The sample layer structures under study are shown in **Figure 1**a, together with X-ray diffraction (XRD) curves in Figure 1b, that allowed to precisely determine the thickness of GaN layers in each structure. Sample 1 consists of a ≈1.4 μm-thick AlN buffer on which a 3 nm unintentionally doped (UID) GaN layer and a 10 nm Mg doped GaN contact layer ([Mg] ≈7×10^{18} cm^{-3}) were grown. Sample 2 is a similar structure, albeit with a thicker ≈2 μm AlN buffer and a 34 nm-thick UID GaN layer on top. The 2DHG is expected at the GaN/AlN interface in both these samples. Room-temperature Hall effect measurements confirm the presence of 2DHGs with densities ≈5×10^{13} cm^{-2} and hole mobilities 11.7 and 9.9 cm^2 Vs^{-1} in sample 1 and 2, respectively. **Figure 2**a shows the CER spectrum measured for sample 1—the Mg:GaN-capped 2DHG structure. The signature of an FKO is clearly visible in the CER data (with its extrema numbered), however, with an additional superimposed oscillatory feature that degrades the CER signal quality. The extra oscillation results from a large difference in refractive indices at air/III-nitride structure and III-nitride/sapphire interfaces that effectively act as an etalon causing a clear Fabry–Perot (F–P) oscillation to arise in the optical spectrum, a feature commonly observed in optical studies of III-nitrides grown on sapphire[15,16] and other material systems.[17] Regardless, the FKO extrema can be identified in the CER spectra by comparing with an expected FKO line shape,[10] shown in Figure 2a by the red line.

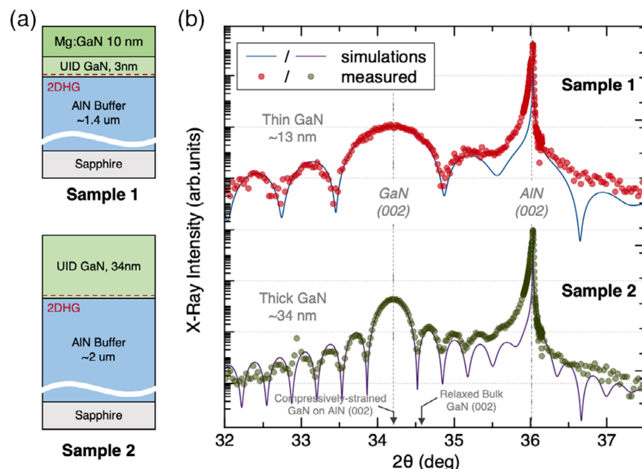

Figure 1. a) Layer structure of the MBE-grown GaN/AlN samples studied in this work. Sample 1 and 2 differ in thicknesses of the layers and the presence of Mg-doped GaN cap. The polarization-induced 2D HGs are expected at the GaN/AlN interfaces as indicated. b) XRD scans of samples 1 and 2 show the difference in fringes arising due to the difference in GaN/AlN layer thicknesses. The GaN (002) peak positions also confirm the compressive strain in the GaN layer.

Figure 2b shows the recorded CER spectrum of sample 2, the GaN/AlN structure with no intentional doping. Unlike sample 1, the spectrum showed negligible influence of an F–P oscillation due to a thicker AlN buffer layer, with only slight deformations of the first and second FKO extrema. This made it easier to analyze the FKO extrema and extract the GaN-related built-in electric field accurately.

The built-in electric field in the GaN channel layers of both GaN/AlN structures from the observed FKOs was calculated by extracting the energetic positions of FKO extrema and applying the formula proposed by Aspnes and Studna,[18] who used the asymptotic form of the Airy function.

$$\frac{\Delta R}{R} \propto \exp\left[\frac{-2\Gamma\sqrt{E-E_g}}{(\hbar\theta)^{\frac{3}{2}}}\right]\cos\left[\frac{4}{3}\left(\frac{E-E_g}{\hbar\theta}\right)^{\frac{3}{2}}+\varphi\right]\frac{1}{E^2(E-E_g)},\quad (\hbar\theta)^3=\frac{e^2\hbar^2F^2}{2\mu} \tag{1}$$

where $\hbar\theta$ is the electro–optic energy, Γ is the linewidth, φ is an angle, F is the electric field, and μ is the electron–hole-reduced mass of the material.

Figure 3a shows a plot of the subsequent FKO extrema in sample 1 and 2, which are given by (from the cosine term in Equation (1)).

$$n\pi = \frac{4}{3}\left(\frac{E_n-E_g}{\hbar\theta}\right)^{\frac{3}{2}}+\varphi \tag{2}$$

where E_n is the energy of nth extremum and E_g is the GaN bandgap energy. The slope of the fitted line through the plot of $4/(3\pi)(E-E_g)^{3/2}$ versus n is proportional to the built-in electric field. The extracted electric field values in the GaN layers are ≈1500 and ≈600 kV cm^{-1} for Sample 1 and 2, respectively. The obtained values of electric fields scale inversely with GaN channel thickness, as the ratios of fields (1500/600 = 2.5) and thicknesses (34/13 = 2.61) are roughly equal. This is expected if the Fermi level is at the same energy at the surface for both samples. The effect of strain through piezoelectric polarization difference is expected to be negligible because both the samples show a similar compressive strain in the GaN layer, as shown in the XRD scan in Figure 1b.

Under this reasoning, further analyses allow the extraction of the Fermi-level position at the surface or the (hole) surface barrier height. The surface barrier is a parameter of particular interest as samples 1 and 2 differ in the doping of the GaN surface exposed to air. To determine the surface barriers, the electric field in the GaN region versus the surface barrier was calculated

 © 2021 Wiley-VCH GmbH

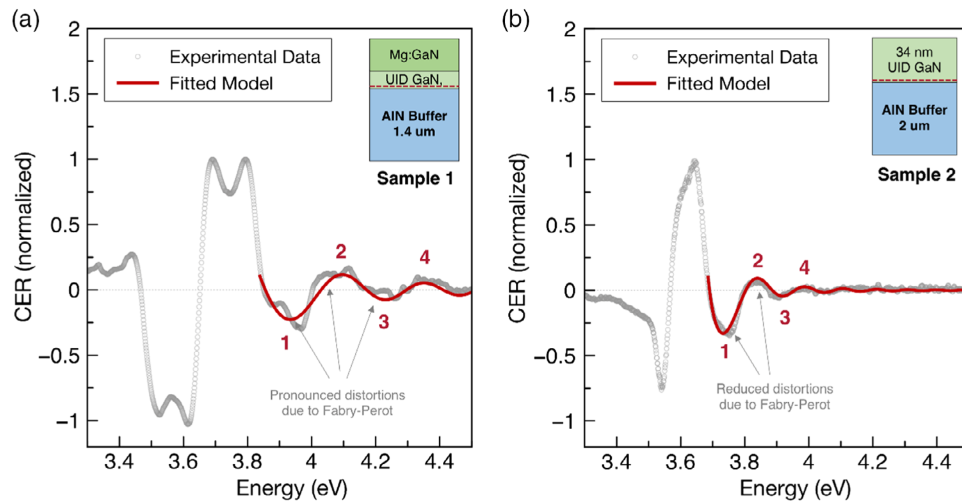

Figure 2. a) CER spectra recorded for the 2DHG sample 1. The numbers indicate the FKO extrema originating from a high electric field in the top GaN layer. In sample 1, peak distortions due to an additional F–P oscillation component are seen. The corresponding extrema are numbered by comparing with a calculated spectrum of $\Delta\varepsilon$ according to Equation (1). b) CER spectra and FKO extraction for sample 2. Thicker epitaxial layers reduce the FPO influence on the CER spectra, and the labeled peaks are clearly visible for further extraction.

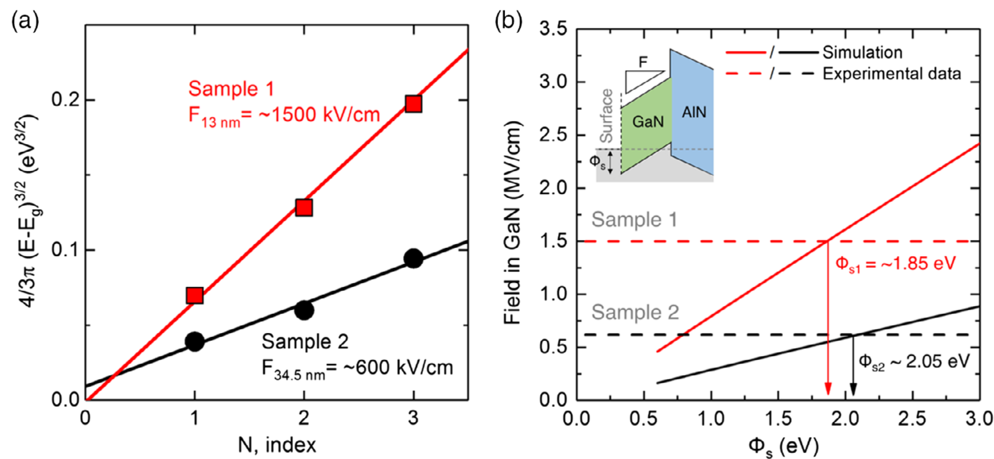

Figure 3. a) Analysis of the built-in electric field due to polarization in sample 1 and 2. The difference in the extracted electric field values between the two samples is attributed to the thickness of GaN layers in structures. Sample 1 with 13 nm of GaN shows a higher built-in field of $\approx$1.5 MV cm^{-1}. b) Calculated dependence of the GaN channel built-in electric field versus surface barrier height (solid lines) compared with experimentally obtained field values (dashed lines) of GaN/AlN structures under study. Crossings of these lines give the extracted surface barrier for each structure—1.85 eV for sample 1 and 2.05 eV for sample 2 (with respect to the VB edge of GaN).

using a self-consistent 1D Schrödinger–Poisson model in nextnano++ solver.[19] Standard material parameters of bandgaps and band offsets (GaN/AlN $\Delta E_V = 0.81$ eV)[20,21] were used, and other experimental parameters (thickness and doping levels) were kept constant and consistent with the nominal values. The GaN layer was assumed to be pseudomorphically strained to the AlN buffer, consistent with the experimental XRD results. The only potential defined in these calculations was the surface barrier height. The band profile landscape in the AlN layer resulted only from the presence of the GaN/AlN interface and an unintentional background dopant density of 10^{16} cm^{-3}. The resulting simulation lines (solid) are shown in Figure 3b and set together with the experimentally obtained built-in electric field values shown as horizontal lines (dashed). The crossing of these lines yields the surface barrier of $\approx$1.85 and $\approx$2.05 eV for holes in the VB for samples 1 and 2, respectively. However, taking into account the partial relaxation of the thicker GaN layer and the fact that an F–P oscillation present in the spectra introduces an uncertainty of the extrema position determination, we are inclined to say that for both of the samples, the surface barrier is the same within experimental accuracy.

Furthermore, using the estimated surface barrier as a parameter, band profiles, i.e., the distribution of the built-in electric field in GaN/AlN heterostructures and hole distribution of each

© 2021 Wiley-VCH GmbH

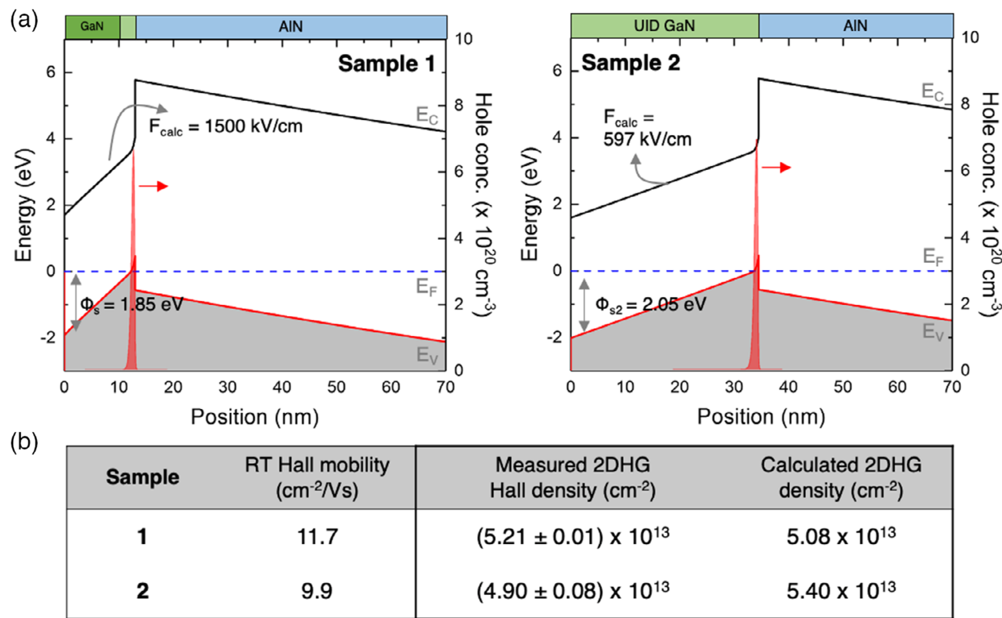

Sample	RT Hall mobility (cm^2/Vs)	Measured 2DHG Hall density (cm^{-2})	Calculated 2DHG density (cm^{-2})
1	11.7	(5.21 ± 0.01) x 10^{13}	5.08 x 10^{13}
2	9.9	(4.90 ± 0.08) x 10^{13}	5.40 x 10^{13}

Figure 4. a) Calculated band profiles and hole concentration profiles of Mg-doped sample 1 and nominally undoped sample 2, zoomed near the GaN/AlN interface where the high-density 2DHGs are expected. The CER extracted surface barrier heights and XRD-confirmed layer thicknesses are used as parameters in the band calculation. b) Room-temperature Hall effect measurement results for samples 1 and 2. A comparison of experimentally obtained 2DHG densities with sheet hole concentrations resulting from the calculation in (a) shows good agreement. This serves as a self-consistent check to lend further confidence to the extracted surface barrier heights for samples 1 and 2.

structure were calculated and are shown in **Figure** 4a. Experimentally obtained values of hole concentration (from Hall effect measurements) are compared with calculated values with a fixed 2.05 eV surface barrier for holes in the Table in Figure 4b. It is shown that calculated 2D hole densities and experimentally measured results agree well to ≈10%. Experimental factors can partly be responsible for the observed differences between experimental and calculated 2DHG densities. From the growth side, factors such as the generation of defects in the films, partial relaxation of the 34 nm-thick GaN layer, and fluctuations in film thicknesses might play a role. Another factor may be the ambiguity of FKO extrema position determination due to distortions induced by the superimposed F–P oscillation and low amplitude of higher-index extrema.

The extracted surface Fermi-level position at ≈1.9 eV above the VB corresponds to one of two theoretically predicted surface states of (0001) GaN,[22,23] that was also observed in air-exposed Ga-polar GaN experimentally.[14] In ultrahigh vacuum conditions, it was also observed that the surface Fermi level can be close to the conduction band or in the middle of the bandgap, depending on the conditions of growth.[24] Generally, studies of GaN surfaces that have been exposed to air ambient always result in a surface barrier height for holes of 2.8–3.1 eV or ≈1.9 eV[14] corresponding to the Fermi level being located in the upper or lower surface state, respectively. The obtained results for GaN/AlN heterostructures in this work correspond well with the latter value, indicating that the Fermi level is in the lower surface state. The importance of this finding lies in the fact that the result is the same for both nominally undoped and Mg-doped structures—Mg doping here does not alter the surface structure. Unlike in the bulk of Mg:GaN layers where the Fermi level can be close to the VB, near the Mg:GaN layer surface in a GaN/AlN structure, the Fermi level is still tied to one of the surface states, at least up to a doping concentration of 7×10^{18} cm^{-3}. This knowledge should be taken into account during the design of (0001) polar GaN/Al(Ga)N structures. In the literature, the Fermi level is fixed at either the upper[25,26] or lower[3,4] GaN surface state for similar calculations of p-channel FET structure band profiles. Some authors, however, use a value that lies in between the two surface states at 2.4 eV above the VB[2] or locate the Fermi level close to the VB edge, presumably at the Mg acceptor level.[1,6] It is thus important to know where to set the surface Fermi-level position for a given structure. In the case of GaN/AlN heterostructures, the large negative interface polarization charge (which is only partially screened by the 2DHG), is evidently strong enough to entirely deplete the electrons from the upper-Fermi pinning surface DOS, thus dropping the surface Fermi level down to the lower pinning states. Magnesium doping only further strengthens this effect. Further work is needed to determine if the surface Fermi level will shift to the upper-surface state above a certain GaN thickness or if any surface treatment will affect the surface barrier.

3. Conclusion

In this work, the built-in electric fields in GaN/AlN heterostructures with 2DHG were studied by CER. FKOs were observed in the CER spectra that allowed to determine the built-in electric field in the GaN channel layers. By solving coupled Schrödinger–Poisson equations and using the obtained GaN

© 2021 Wiley-VCH GmbH

built-in electric field as a parameter, band profiles of the structures were calculated, revealing that the Fermi level is ≈1.9 above the VB for both nominally undoped and Mg-doped structures. This value corresponds to the previously observed lower surface state of (0001) GaN. Calculated 2DHG densities reflect values obtained from Hall effect measurements, further strengthening the findings from optical studies.

4. Experimental Section

Sample Growths: The samples studied in this work were grown using plasma-assisted molecular beam epitaxy (PA-MBE) in a Veeco Gen10 system. The sample layer structures are shown in the Figure 1. Commercially available metal-polar AlN templates, with ≈1 μm of metal–organic chemical vapor deposition-grown AlN on sapphire, were used as the starting substrate. A further AlN buffer was grown by MBE, ≈400 nm for sample 1 and ≈1 μm for sample 2. For the active region, sample 1 had a 3 nm UID GaN with a Mg-doped GaN cap of 10 nm ([Mg] $\approx 7 \times 10^{18}$ cm^{-3}). Sample 2 was kept completely undoped—with the top UID GaN layer thickness of 34 nm. The growth conditions for Mg doping were calibrated using secondary-ion mass spectrometry (SIMS) on a separate reference sample. Further details of the growth are reported elsewhere.[9,27] The quality and thicknesses of the films postgrowth were confirmed using XRD, as shown in Figure 1. Relative peak positions in reciprocal space maps (RSM) around the (105) peak point to the GaN film being compressively strained to AlN on both the samples. Hall effect measurements at 1 T were carried out to confirm the presence of the 2DHG in the samples in a Lakeshore Hall measurement system.

Optical Studies: The CER measurements were carried out at room temperature in air ambient in a so-called dark configuration that allows to minimize the illumination density often detrimental to III-nitride structure studies.[10,28] A beam from the Energetiq EQ-99X laser-driven light source was directed to an Andor Shamrock SR-750 monochromator using reflective optics and then the monochromatic beam was reflected from the sample surface. The signal was detected with a Hamamatsu photomultiplier tube. Samples were placed in a capacitor with one of the electrodes made from a semitransparent copper wire. Other relevant details about the CER setup can be found elsewhere.[29] The subsequent calculations for data analysis and band simulations were carried out in a nextnano++ solver.[19]

Acknowledgements

Ł.J. and R.C. contributed equally to this work. This work was conducted within the OPUS grant of the National Science Centre, Poland (no. 2016/21/B/ST7/01274), also supported partly by Intel Corporation, Air Force Office of Scientific Research (AFOSR grant FA9550-20-1- 0048), and NSF (grants 1710298 and 1534303). Part of this work was conducted at Cornell Nanoscale Facility, an NNCI member supported by NSF Grant NNCI-2025233, and at Cornell Center for Materials Research Shared Facilities, which is supported through the NSF MRSEC program (DMR-1719875) and NSF MRI (DMR-1429155 and DMR-1338010) programs.

Conflict of Interest

The authors declare no conflict of interest.

Data Availability Statement

Research data are not shared.

Keywords

III-nitride heterostructures, Franz–Keldysh oscillations, modulation spectroscopy, surface Fermi levels, two-dimensional hole gases

Received: December 9, 2020
Revised: January 12, 2021
Published online:

[1] M. Shatalov, G. Simin, V. Adivarahan, A. Koudymov, R. Pachipulusu, M. A. Khan, *IEEE Electron Device Lett.* **2002**, *23*, 452.
[2] T. Zimmermann, M. Neuburger, M. Kunze, I. Daumiller, A. Denisenko, A. Dadgar, A. Krost, E. Kohn, in *61st Device Research Conf. Conf. Digest* (Cat. No.03TH8663), IEEE, Salt Lake City, UT, USA **2003**, pp. 19–20, https://doi.org/10.1109/DRC.2003.1226852.
[3] H. Hahn, B. Reuters, A. Pooth, B. Holländer, M. Heuken, H. Kalisch, A. Vescan, *IEEE Trans. Electron Devices* **2013**, *60*, 3005.
[4] B. Reuters, H. Hahn, A. Pooth, B. Holländer, U. Breuer, M. Heuken, H. Kalisch, A. Vescan, *J. Phys. D: Appl. Phys.* **2014**, *47*, 175103.
[5] A. Nakajima, S. Nishizawa, H. Ohashi, H. Yonezawa, K. Tsutsui, K. Kakushima, H. Wakabayashi, H. Iwai, in *2014 IEEE 26th Int. Symp. Power Semiconductor Devices IC's (ISPSD)*, IEEE, Piscataway, NJ, USA **2014**, pp. 241–244, https://doi.org/10.1109/ISPSD.2014.6856021.
[6] K. Zhang, M. Sumiya, M. Liao, Y. Koide, L. Sang, *Sci. Rep.* **2016**, *6*, 23683.
[7] K. Nomoto, R. Chaudhuri, S. J. Bader, L. Li, A. Hickman, S. Huang, H. Lee, T. Maeda, H. W. Then, M. Radosavljevic, P. Fischer, A. Molnar, J. C. M. Hwang, H. G. Xing, D. Jena, in *2020 IEEE International Electron Devices Meeting (IEDM)*, IEEE, Piscataway, NJ, USA **2020**.
[8] S. J. Bader, R. Chaudhuri, A. Hickman, K. Nomoto, S. Bharadwaj, H. W. Then, H. G. Xing, D. Jena, in *2019 IEEE Int. Electron Devices Meeting (IEDM)*, IEEE, Piscataway, NJ, USA **2019**, https://doi.org/10.1109/IEDM19573.2019.8993532.
[9] R. Chaudhuri, S. J. Bader, Z. Chen, D. A. Muller, H. G. Xing, D. Jena, *Science* **2019**, *365*, 1454.
[10] H. Shen, M. Dutta, *J. Appl. Phys.* **1995**, *78*, 2151.
[11] C. V. Hoof, K. Deneffe, J. D. Boeck, D. J. Arent, G. Borghs, *Appl. Phys. Lett.* **1989**, *54*, 608.
[12] R. Kudrawiec, M. Gladysiewicz, L. Janicki, J. Misiewicz, G. Cywinski, C. Chèze, P. Wolny, P. Prystawko, C. Skierbiszewski, *Appl. Phys. Lett.* **2012**, *100*, 181603.
[13] R. Kudrawiec, H. P. Nair, M. Latkowska, J. Misiewicz, S. R. Bank, W. Walukiewicz, *J. Appl. Phys.* **2012**, *112*, 123513.
[14] Ł. Janicki, M. Gładysiewicz, J. Misiewicz, K. Klosek, M. Sobanska, P. Kempisty, Z. R. Zytkiewicz, R. Kudrawiec, *Appl. Surf. Sci.* **2017**, *396*, 1657.
[15] A. Rizzi, M. Kocan, J. Malindretos, A. Schildknecht, N. Teofilov, K. Thonke, R. Sauer, *Appl. Phys. A* **2007**, *87*, 505.
[16] M. Motyka, R. Kudrawiec, M. Syperek, J. Misiewicz, M. Rudziński, P. R. Hageman, P. K. Larsen, *Thin Solid Films* **2007**, *515*, 4662.
[17] M. Wełna, R. Kudrawiec, J. Misiewicz, M. Yano, K. Koike, S. Sasa, *Phys. Status Solidi A* **2015**, *212*, 780.
[18] D. E. Aspnes, A. A. Studna, *Phys. Rev. B* **1973**, *7*, 4605.
[19] S. Birner, T. Zibold, T. Andlauer, T. Kubis, M. Sabathil, A. Trellakis, P. Vogl, *IEEE Trans. Electron Devices* **2007**, *54*, 2137.
[20] S. Wei, A. Zunger, *Appl. Phys. Lett.* **1996**, *69*, 2719.
[21] A. Bhouri, J.-L. Lazzari, *Mater. Sci. Semicond. Process.* **2016**, *41*, 121.
[22] D. Segev, C. G. V. de Walle, *Europhys. Lett.* **2006**, *76*, 305.
[23] M. Himmerlich, L. Lymperakis, R. Gutt, P. Lorenz, J. Neugebauer, S. Krischok, *Phys. Rev. B* **2013**, *88*, 125304.
[24] M. Kočan, A. Rizzi, H. Lüth, S. Keller, U. K. Mishra, *Phys. Status Solidi B* **2002**, *234*, 773.

© 2021 Wiley-VCH GmbH

[25] S. J. Bader, R. Chaudhuri, K. Nomoto, A. Hickman, Z. Chen, H. W. Then, D. A. Muller, H. G. Xing, D. Jena, *IEEE Electron Device Lett.* **2018**, *39*, 1848.
[26] A. Nakajima, S. Kubota, K. Tsutsui, K. Kakushima, H. Wakabayashi, H. Iwai, S. Nishizawa, H. Ohashi, *IET Power Electron.* **2018**, *11*, 689.
[27] R. Chaudhuri, S. J. Bader, Z. Chen, D. Muller, H. G. Xing, D. Jena, *Phys. Status Solidi B* **2020**, *257*, 1900567.
[28] Ł. Janicki, J. Misiewicz, M. Siekacz, H. Turski, J. Moneta, S. Gorantla, C. Skierbiszewski, R. Kudrawiec, *Sens. Actuators B* **2019**, *281*, 561.
[29] R. Kudrawiec, *Phys. Status Solidi B* **2010**, *247*, 1616.

© 2021 Wiley-VCH GmbH